Biomedical Materials & Devices (2023) 1:504–511
https://doi.org/10.1007/s44174-022-00017-0

ORIGINAL PAPER

Polymer Sponge Replication Technology Derived Strontium-Substituted Apatite (Sr-HAP) Porous Scaffolds for Bone Tissue Engineering

Ramadas Munusamy[1] · Abimanyu Ravichandran[1] · Khalil El Mabrouk[2] · Ballamurugan M. Anbalagan[1]

Received: 2 April 2022 / Accepted: 8 August 2022 / Published online: 31 August 2022

Abstract

In this research, we developed strontium-substituted apatite (Sr-HAP) scaffolds using the polymeric sponge replication method. Tissue engineering is a potential new technology for replacing damaged tissue with biocompatible artificial templates. The scaffolds prepared with an interconnected porous microstructure with pore sizes ranging from 400 to 622 µm were created as engineering constructions. The physicochemical properties of the Sr-HAP scaffolds were characterized by various techniques such as X-ray diffraction (XRD), Field emission scanning electron microscopy (FE-SEM), and Energy dispersion spectroscopy (EDS). Immersion tests in simulated body fluid (SBF) solution was used to assess the surface reactivity of the resulting scaffolds. More critically, MTT assay tests were utilized to investigate the cell viability of porous Sr-HAP scaffold at varying doses of 10–1000 µg/mL for 24 h. The porosity Sr-HAP scaffolds developed in this study are a potential tissue engineering candidate.

Graphical Abstract

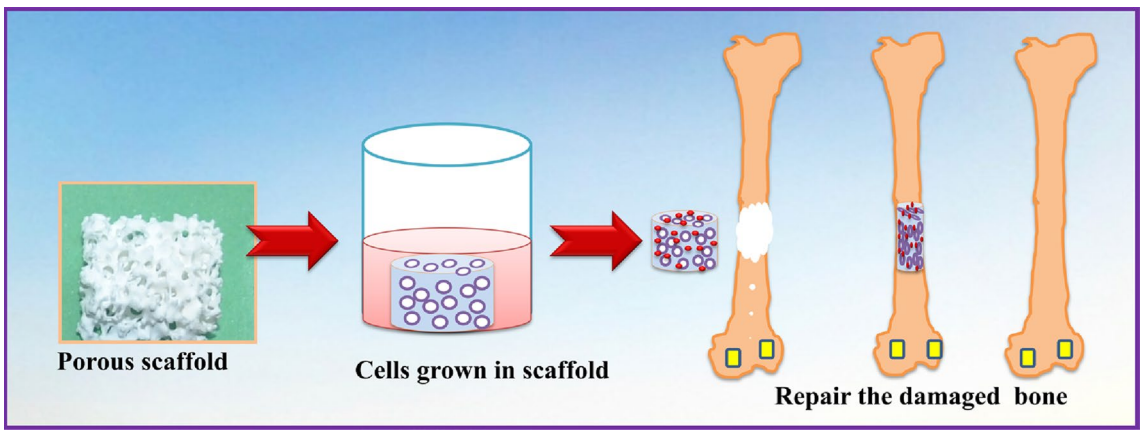

Keywords Apatite · Porous · Scaffold · Biocompatibility · Tissue engineering

Introduction

Accidental bone defects and fractures, as well as skeletal disorders and tumour resections, have become a worldwide problem and clinical concern. Tissue engineering and regenerative medicine have been establishing their potential value to transform critical fields of medicine,

✉ Ballamurugan M. Anbalagan
balamurugan@buc.edu.in

[1] Department of Nanoscience and Technology, Bharathiar University, Coimbatore, Tamil Nadu 641046, India

[2] Euromed Engineering Faculty, Université Euromed de Fès, BP 51, Fès principale, Fès, Morocco

such as bone treatment, artificial skin, and cardiovascular, since the 1980s and especially in the last decade [1, 2]. Tissue engineering is a method that combines biological features like growth with engineering concepts and synthetic materials to build new tissue [3, 4]. The temporary three-dimensional (3D) scaffolds play a crucial role in the modification of osteoblast functions and the steering of new bone formation into desired shapes in the tissue engineering technique [5]. Scaffolds must have strong biocompatibility to avoid immunological rejection by the host, osteoconduction capacity to help bone regeneration, and appropriate mechanical qualities to provide mechanical compatibility with surrounding tissues [6]. The ability of cells to differentiate, proliferate and penetrate as well as the pace of scaffold disintegration, is greatly influenced by the pore distribution and shape of the scaffold [7]. These inorganic compounds of hydroxyapatite (HAP), biphasic calcium phosphate (BCP) and beta tricalcium phosphate (β-TCP) materials are used in a variety of biomedical applications, including dental and orthoptics surgery [8–10]. Synthetic apatite (HAP) has been one of the biomaterials most commonly utilized to make scaffolds because of its remarkable osteophilic property and a great likeness to the mineral component of bone [11]. As a result, the crystal phase and functional group of apatite (HAP) allow for a wide range of substitutions, such as Mg, Sr, Zn, Si, and Mn as Ca substitutes, which have been used to achieve excellent mechanical strength and biocompatibility [12, 13]. Strontium (Sr) is widely known for its function in remodelling; it stimulates bone synthesis and reduces bone resorption [14]. These are research on tissue engineering with created porous scaffolds and various techniques. Developed porous scaffolds are made variously of techniques, including gel-casting, freeze-casting, foam-casting, and 3D printing [15–18]. Polymeric sponge replication has recently been demonstrated as a promising and successful technology for producing scaffolds with density, good macropore interconnectivity, open porosity and pore size similar to cancellous bone [19, 20].

In this work, the fabrication of strontium-substituted apatite (Sr-HAP) scaffolds for bone tissue engineering. The PP120 type of polymer sponge was square shaped into a slurry with 30% solid load and 20% organic binder to create polymer sponge replication techniques. The benefit of this approach is that it permits a high degree in the interconnected porous structure, pore size and biological degradation of 3D scaffolds. The structure and physicochemical properties are characterized by X-ray diffraction and field emission scanning electron microscopy. In vitro bioactive and biocompatibility of Sr-HAP scaffolds were was evaluated by using simulated body fluid (SBF) and MG-63 cell lines studies. The Sr-HAP scaffolds with interconnected porosity might be employed in bone tissue engineering.

Experimental Methods

Chemicals and Reagents

Calcium nitrate ($Ca(NO_3)_2{\cdot}4H_2O$; SDFCL, India), strontium nitrate ($Sr(NO_3)_2$; SDFCL, India), di-ammonium hydrogen phosphate ($(NH_4)_2HPO_4$; SDFCL, India), ammonium hydroxide solution (NH_4OH; SDFCL, India), *N,N,N′N′*-tetramethylethylenediamine-TEMED (Thomas scientific, India), polyvinyl alcohol-PVA (SDFCL, India) and *N,N′*-methylenebisacrylamide-MBA (Thomas scientific, India). All of the compounds were analytical grade and were not purified before use.

Preparation of Sr-Substituted HAP

The synthesis of Sr-substituted HAP powders with a molar ratio of (Ca + Sr)/P was equal to stoichiometric value (0.98 + 0.02/0.6 = 1.666) of were made by simple precipitation. Then 0.98 mol of calcium nitrate ($Ca(NO_3)_2{\cdot}4H_2O$) was dissolved in 250 mL of double distilled water and 0.6 mol amount of di-ammonium hydrogen phosphate ($(NH_4)_2HPO_4$) mixtures was added to the cationic and anionic solutions, under stirring for a period of 30 min by a stirring condition 200 rpm. After complete dissolution, the 0.02 mol of strontium nitrate ($Sr(NO_3)_2$) was added gradually to cationic solution and continue stirring room temperature. The pH was adjusted to 10.5 by drop wise drop addition 1 mol of ammonium hydroxide (NH_4OH) solution with vigorous stirring for 30 min. The precipitates solution was magnetic stirred for 2 h and then separated through filtration technique and dried in the oven at 80 °C for 24 h. As a result, dried powders were heat-treated for 2 h at 800 °C before being crushed in a planetary ball mill (Retsch, Germany) to reduce particle size and fine-filtered through a 75 μm screen [21, 22].

Fabrication of Three-Dimensional (3D) Scaffolds

The scaffolds were made using a combination of gel-casting and polymeric sponge replication methods (Fig. 1). To make slurries with a solid load of 30%, the gel-casting technique was used, which involved dispersing Sr-HAP in an aqueous solution containing 20% organic polymers binder (polyvinyl alcohol-PVA), crosslinker (*N,N′*-methylenebisacrylamide-MBA) and dispersant (*N,N,N′N′*-tetramethylethylenediamine-TEMED) in a 3:3:1 mol. Ball-milling (Retsch planetary) has been used to deagglomerate the prepared slurry for 48 h at 600 rpm. After the slurry had been prepared, the polymer sponge (PP120 type) suspension was infiltrated. To remove all volatile contaminants, the dried sample was heated to 800 °C with a heating rate

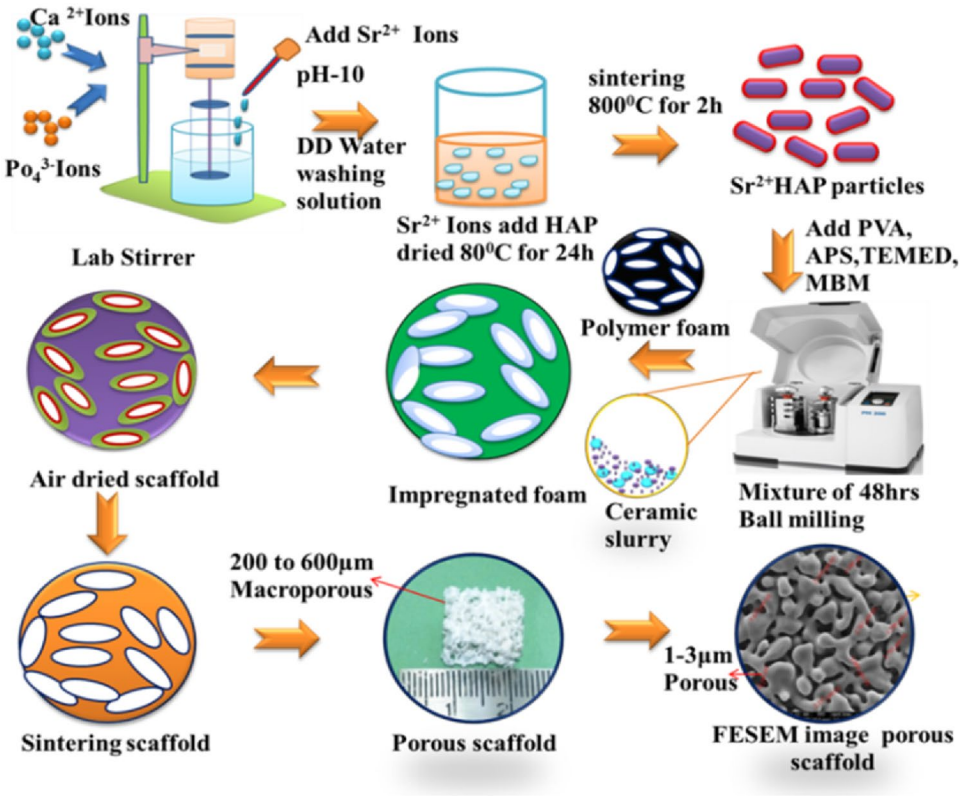

Fig. 1 Schematic representation of HAP and Sr-HAP scaffolds by polymeric sponge replication method

of 1 °C min and a dwell time of 90 min. Following that, the temperature was raised to 1000 °C to 1200 °C with a 1 °C/min heating rate and a 2 h well time [23, 24].

Physicochemical Characterization of Scaffolds

X-ray Diffraction (XRD)

The crystal phase and structure of the fabricated Sr-HAP scaffolds were investigated X-ray diffraction (XRD). A Bruker AXSD-8 advance X-ray diffraction was used for the measurement, which was done at ($\lambda = 1.5406$ Å) using monochromatic CuK α radiation. Dates were collected at a scan rate of 0.1° min^{-1} form two theta (2θ) range of 2060°.

Field Emission Scanning Electron Microscopy (FE-SEM)

The microstructure analysis was obtained by using scanning electron microscopy (Model: FE-SEM-FEI Quanta-250 FEG) with accelerating voltage 200 V to 15 K V. To avoid charging, a small layer of gold was sprayed onto the porous scaffolds' surfaces using an ion sputtering instrument.

In vitro Tests of Scaffolds in a SBF

In vitro testing was done on the bioactivity of the apatite (HAP) and Sr-substituted apatite (Sr-HAP) scaffolds in simulated body fluid. The simulated body fluid solution was made by combining 142.0 mM NaCl, 4.2 mM $NaHCO_3$, 5.0 mM KCl, 1.0 mM $K_2HPO_4{\cdot}3H_2O$, 1.5 mM $MgCl_2{\cdot}6H_2O$, 2.5 mM $CaCl_2$, and 0.5 mM Na_2SO_4 (Merck, India) which buffered at pH 7.4 ± 2 with [$(CH_2OH)_3CNH_3$; Merck, India] and hydrochloric acid (HCl; Merck, India). After 3, 7 and 14 days of immersion in a 50 mL simulated body fluid (SBF) solution, samples were withdrawn from the SBF, gently washed with double distilled water, dried at room temperature and surface reactivity of characterized [25].

In Vitro Cell Line Studies

Cell Culture Reagents

MG-63 cell lines (National Centre for Cell Science (NCC), Pune, Maharashtra and India). 3-(4,5-dimethylthiazol-2-yl)-2,5-diphenyltetrazolium bromide-MTT (Bio Basic Canada Inc, Canada). Dulbecco's modified eagle's medium-DMEM (Sigma-Aldrich, India), Penicillin-PEN (Sigma-Aldrich, India), Foetal bovine serum-FBS (Sigma-Aldrich, India) and phosphate buffer saline–PBS (Sigma-Aldrich, India). All of the compounds were analytical grade and were not purified before use.

Cell Viability Study on the Scaffold

The MG-63 cell line was approved for use in this study by the National centre for cell science (NCC) in Pune, Maharashtra, India. The MG-63 cells were grown in Dulbecco's Modified Eagles Medium (DMEM) which included 1% penicillin, 10% foetal bovine serum (FBS), and 10% streptomycin sulphate. The cell lines were maintained at 37 °C in a 5% CO_2 atmosphere, with the medium changed every three days. The cell lines were seeded at a density of 1×10^4 cells per well in 96-well plates and then treated for 24 h with 100 µL of complete culture media in the negative and positive control of a series of escalating concentrations of 10, 30, 100, 300, and 1000 g/mL of scaffolds. The absorbance of the coloured solution at a wavelength of 570 nm can be measured using a microplate absorbance spectrophotometer [26].

Results and Discussion

X-ray Diffraction (XRD) Analysis

The X-ray diffraction patterns of the samples obtained suggested that they were pure HAP and Sr-HAP crystal phase Fig. 2i(a and b). The characteristic peaks at 2θ = 25.53, 28.63, 31.51, 32.58, 39.48, 46.11, and 48.85° correspond to the (002), (211), (112), (300), (310), (222), and (004) planes, verifying the hexagonal structure. The predominant crystal phase was HAP, and the strong peak in the patterns showed good coincidence. However, no distinct peaks were detected for Sr-HAP compared to apatite (HAP), implying that the Sr substitution in the apatite matrix has no significant effect on the crystalline phase due to the low concentration of Sr ions.

Figure 2ii(a and b) shows the XRD patterns of the three-dimensional (3D) porous Sr-HAP scaffolds prepared at 1000 °C and 1200 °C which displays the reflection of crystal phase. The prominent peaks in the spectrum are $2\theta = 21.71$, 25.75, 27.76, 28.84, 30.96, 32.44, 34.31, 46.90, and 52.95 corresponding to (200), (002), (214), (210), (211), (300), (220), (222), and (213) which exactly matched with the (JCPDS card no. 09–0432) for apatite (HAP) and 09-0169 for β-tricalcium phosphate (β-TCP) mixture of crystal phase. These findings suggest that high-pore scaffolds can be sintered and densified at 1200 °C without the production of other calcium phosphate crystalline phases other than apatite [27].

FE-SEM and EDS Analysis

Figure 3a–c shows the morphological investigation of apatite (HAP) and Sr-substituted apatite (Sr-HAP) using field emission scanning electron microscopy (FE-SEM). The typical size of HAP is estimated to be between 100 and 150 nm, with greater agglomeration due to Sr substitution. Figure 3d presents that calcium (Ca), oxygen (O), strontium (Sr), phosphate (P), and carbon (C) elements are visible in the EDS spectra of the powder in the as-dried conditions. Figure 4a shows an optical image of interconnected pore structures in a three-dimensional Sr-HAP scaffold. In Figure 4b and c, after sintering at 1200 °C for 2 h, the scaffold was shaped into a square shape with a diameter of 4.5 cm 4.56 cm, which was sufficient for a conditioned biological habitat. The macropores have pore diameters ranging from 400 to 622 µm, and produced utilizing the polymer sponge process. The pore shape of a Sr-HAP scaffold for tissue regeneration should be restricted to facilitate proliferation and cell migration. Furthermore, the scaffold's pore size is likely to play an

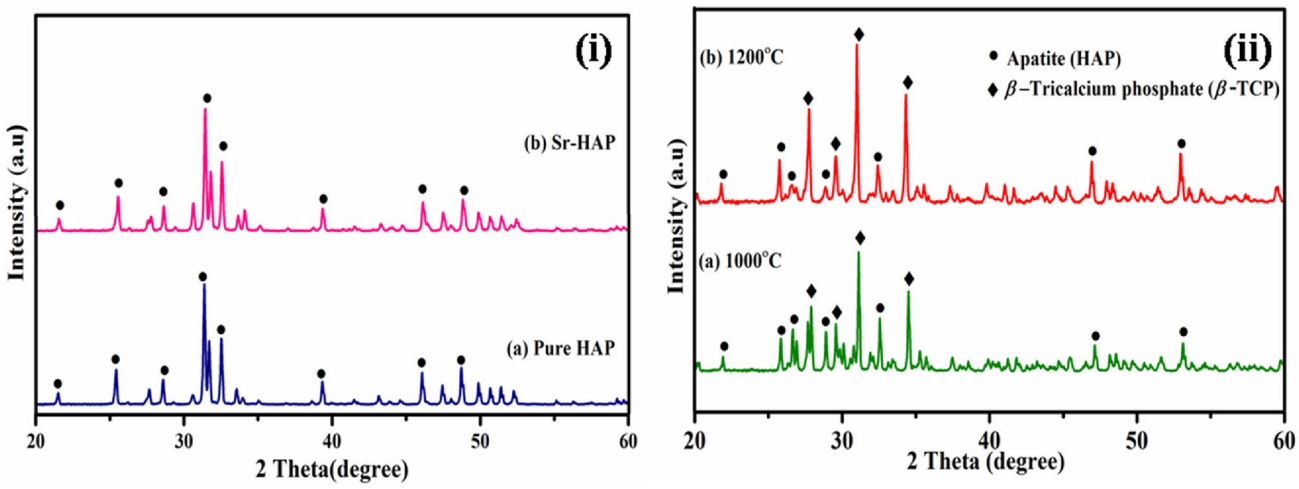

Fig. 2 XRD patterns for **i** HAP and Sr-HAP powders and **ii** pure HAP and Sr-HAP scaffold after heat treatment at 1000 °C and 1200 °C

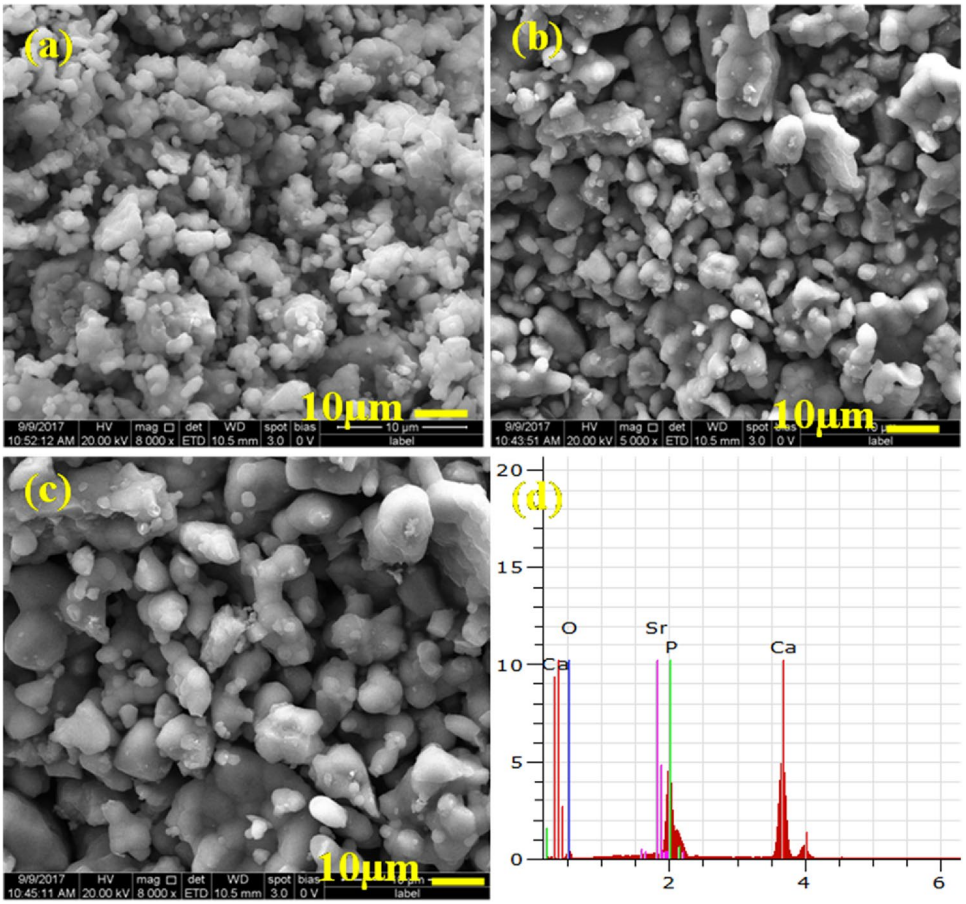

Fig. 3 FE-SEM morphology of **a** and **b** pure HAP, **c** Sr-HAP and **d** EDS spectrum of Sr-HAP powder

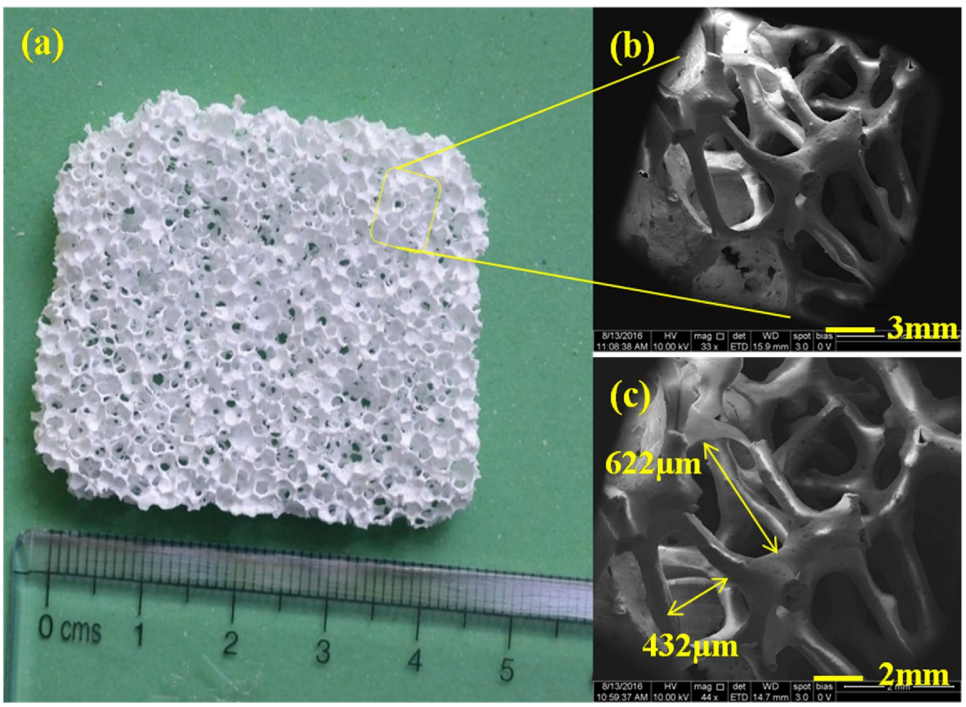

Fig. 4 Optical image of scaffold after sintering and FE-SEM morphology of HAP and Sr-HAP porous scaffolds obtained through polymeric sponge replication method

essential role in tissue engineering since they have a higher proclivity for providing room for cell uptake [28].

In Vitro Bioactivity of SBF Studies

The in vitro bioactivity analysis of the pure HAP and Sr-HAP scaffolds was assessed by immersing the samples in SBF solution for various times, respectively (Fig. 5). After three days of immersion, the surface of pure HAP and Sr-HAP scaffolds showed deposition of small amount of calcium phosphate granules, as shown in Fig. 5. The bone-like HAP crystallites grew and were spared over on the surface of both discs after seven days of soaking in SBF (Fig. 5b). For both samples, there was a rapid rise in HAP precipitation when the incubation duration was extended. The carbonate apatite layer had entirely covered the surface of the scaffolds after 14 days of immersion. The results show that the manufactured porous scaffold has outstanding bioactivity, implying that the created scaffolds are well suited to tissue engineering [29].

In Vitro Cell Viability Studies

To investigate bioactivity, MG-63 cell lines were grown for 24 h on pure HAP and Sr-HAP scaffolds at concentrations ranging from 10 to 1000 µg/mL (Fig. 6). For concentrations of 10 and 1000 g/mL, respectively, cell viability was significantly reduced to pure 92 and 46 percent (%) in the MTT assay. With increasing concentrations of pure HAP and

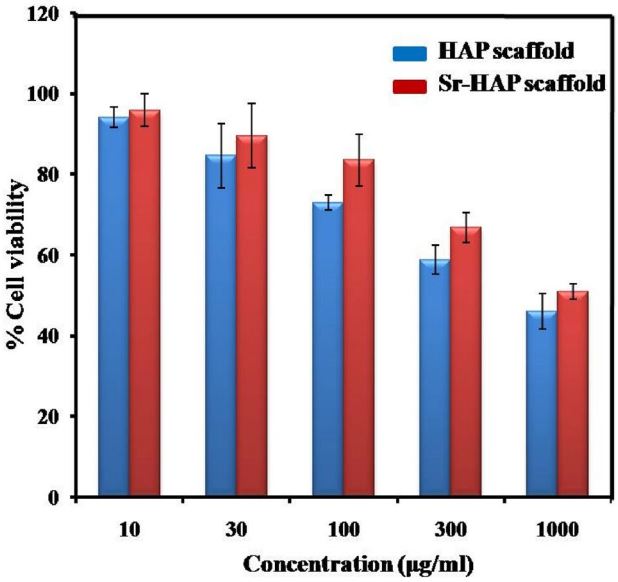

Fig. 6 In vitro cell viability analysis of HAP and Sr-HAP scaffolds for different concentrations (10 to 1000 µg/mL) to MG-63 cells at 24 h

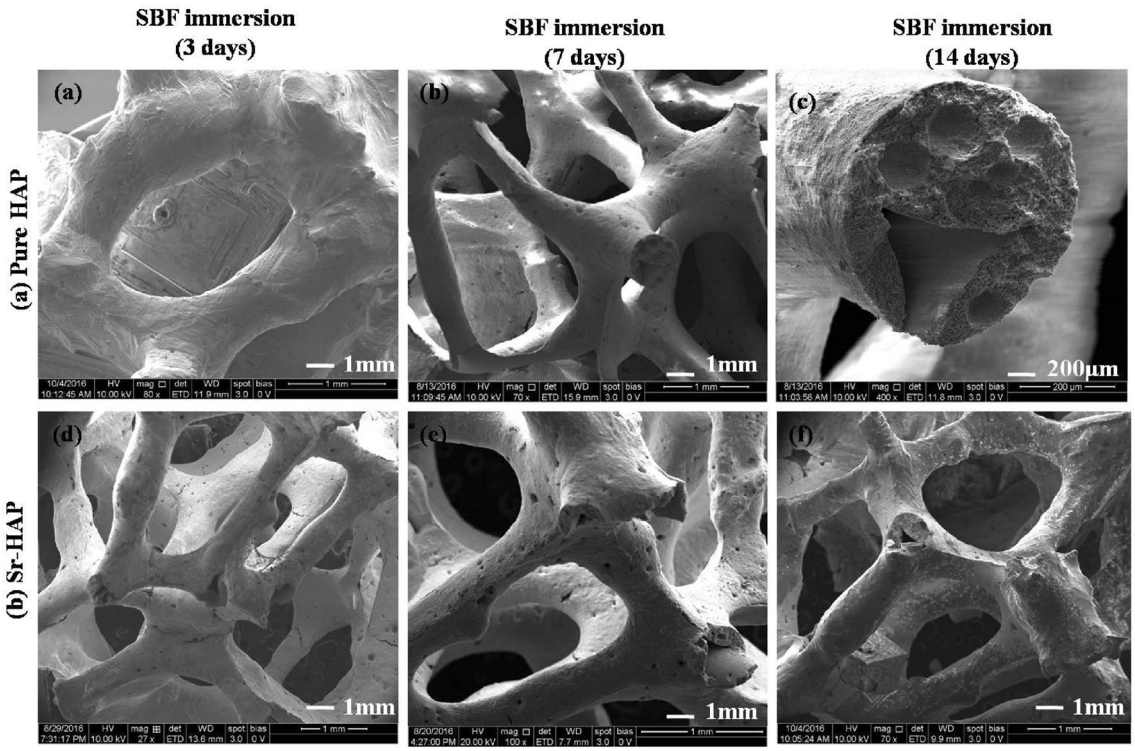

Fig. 5 FE-SEM image scaffold porous **a** HAP scaffold and **b** Sr-HAP scaffold prior to SBF immersion experiments. Soaking by SBF solution **a**–**f** 3, 7 and 14 days immersion test

Sr-HAP scaffolds, cell viability declines gradually. These characteristics demonstrated that the porous scaffolds system is capable of tissue engineering [30].

Summary

A new method for fabricating three-dimensional Sr-HAP scaffolds for tissue regeneration using a combination of gel-casting and polymer sponge technology has been devised. In the Sr-HAP scaffolds, researchers discovered interconnected pore diameters ranging from 400 to 622 µm structures, osteoconductivity improved physio-mechanical properties. The biological response of the Sr-HAP scaffold was investigated using simulated body fluid (SBF) and MG-63 cell lines test. As a result, the evolution of porous Sr-HAP scaffolds for future medicinal applications in tissue regeneration has produced a more acceptable option.

Acknowledgements This work supported authors are grateful to ICMR-RA No.45/79/2018-Nan/BMS, New Delhi-India for the financial support and for the research Project Support TNSCST/STP-PRG/AR/2018-19/9282 Chennai, Tamil Nadu, India.

Declarations

Conflict of interest The authors declare that they have no known competing financial interests or personal relationships that could have appeared to influence the work reported in this paper.

References

1. S. Bajada, I. Mazakova, J.B. Richardson, N. Ashammakhi, Updates on stem cells and their applications in regenerative medicine. J. Tissue Eng. Regen. Med. **2**, 169–183 (2008). https://doi.org/10.1002/term.83
2. S.A. Sell, M.J. McClure, K. Garg, P.S. Wolfe, G.L. Bowlin, Electrospinning of collagen/biopolymers for regenerative medicine and cardiovascular tissue engineering. Adv. Drug Deliv. Rev. **61**, 1007–1019 (2009). https://doi.org/10.1016/j.addr.2009.07.012
3. P. Zhao, H. Gu, H. Mi, C. Rao, J. Fu, L.S. Turng, Fabrication of scaffolds in tissue engineering: a review. Front. Mech. Eng. **13**, 107–119 (2018). https://doi.org/10.1007/s11465-018-0496-8
4. M. Okamoto, B. John, Synthetic biopolymer nanocomposites for tissue engineering scaffolds. Prog. Polym. Sci. **38**, 1487–1503 (2013). https://doi.org/10.1016/j.progpolymsci.2013.06.001
5. L. Kumar, D. Ahuja, Preparation and characterization of aliphatic polyurethane and modified hydroxyapatite composites for bone tissue engineering. Polym. Bull. **77**, 6049–6062 (2020). https://doi.org/10.1007/s00289-019-03067-5
6. X. Song, H. Tetik, T. Jirakittsonthon, P. Parandoush, G. Yang, D. Lee, D. Lin, Biomimetic 3D printing of hierarchical and interconnected porous hydroxyapatite structures with high mechanical strength for bone cell culture. Adv. Eng. Mater. **21**, 1800678 (2019). https://doi.org/10.1002/adem.201800678
7. G.H. Billström, A.W. Blom, S. Larsson, A.D. Beswick, Application of scaffolds for bone regeneration strategies: current trends and future directions. Injury **44**, S28–S33 (2013). https://doi.org/10.1016/S0020-1383(13)70007-X
8. A. De Luca, I. Vitrano, V. Costa, L. Raimondi, V. Carina, D. Bellavia, G. Giavaresi, Improvement of osteogenic differentiation of human mesenchymal stem cells on composite poly L-lactic acid/nano-hydroxyapatite scaffolds for bone defect repair. J. Biosci. Bioeng. **129**, 250–257 (2020). https://doi.org/10.1016/j.jbiosc.2019.08.001
9. R.W.N. Nilen, P.W. Richter, The thermal stability of hydroxyapatite in biphasic calcium phosphate ceramics. J. Mater. Sci. Mater. Med. **19**, 1693–1702 (2008)
10. J. Diao, J. OuYang, T. Deng, X. Liu, Y. Feng, N. Zhao, Y. Wang, 3D-plotted beta-tricalcium phosphate scaffolds with smaller pore sizes improve in vivo bone regeneration and biomechanical properties in a critical-sized calvarial defect rat model. Adv. Healthc. Mater. **7**, 1800441 (2018). https://doi.org/10.1002/adhm.201800441
11. K.F. Lin, S. He, Y. Song, C.M. Wang, Y. Gao, J.Q. Li, G.X. Pei, Low-temperature additive manufacturing of biomimic three-dimensional hydroxyapatite/collagen scaffolds for bone regeneration. ACS. Appl. Mater. Interfaces **8**, 6905–6916 (2016). https://doi.org/10.1021/acsami.6b00815
12. M. Ramadas, V. Nivedha, K. Eimabrouk, A.M. Ballamurugan, Impact and biocompatibility studies on Mg^{2+}-substituted apatite-derived 3D porous scaffolds for hard tissue engineering. Int. J. Appl. Ceram. Technol. **16**, 1962–1968 (2019)
13. C. Garbo, J. Locs, M. D'Este, G. Demazeau, A. Mocanu, C. Roman, M. Tomoaia-Cotisel, Advanced Mg, Zn, Sr, Si multi-substituted hydroxyapatites for bone regeneration. Int. J. Nanomed. **15**, 1037 (2020). https://doi.org/10.2147/IJN.S226630
14. R. Zhao, S. Chen, W. Zhao, L. Yang, B. Yuan, V.S. Ioan, X. Zhang, A bioceramic scaffold composed of strontium-doped three-dimensional hydroxyapatite whiskers for enhanced bone regeneration in osteoporotic defects. Theranostics **10**, 1572 (2020)
15. M. Ramadas, K. EI Mabrouk, A.M. Ballamurugan, Apatite derived three dimensional (3D) porous scaffolds for tissue engineering applications. Mater. Chem. Phys. **242**, 122456 (2020). https://doi.org/10.1016/j.matchemphys.2019.122456
16. H. Lee, T.S. Jang, J. Song, H.E. Kim, H.D. Jung, The production of porous hydroxyapatite scaffolds with graded porosity by sequential freeze-casting. Materials **10**, 367 (2017). https://doi.org/10.3390/ma10040367
17. X. Wang, J.H. Li, Y.M. Xie, H.Y. Zhang, Three-dimensional fully interconnected highly porous hydroxyapatite scaffolds derived from particle-stabilized emulsions. Ceram. Int. **42**, 5455–5460 (2016). https://doi.org/10.1016/j.ceramint.2015.12.088
18. H. Sun, C. Zhang, B. Zhang, P. Song, X. Xu, X. Gui, X. Zhang, 3D printed calcium phosphate scaffolds with controlled release of osteogenic drugs for bone regeneration. Chem. Eng. J. **427**, 130961 (2022). https://doi.org/10.1016/j.cej.2021.130961
19. Z. Dong, Y. Li, Q. Zou, Degradation and biocompatibility of porous nano-hydroxyapatite/polyurethane composite scaffold for bone tissue engineering. Appl. Surf. Sci. **255**, 6087–6091 (2009). https://doi.org/10.1016/j.apsusc.2009.01.083
20. S.M. Imani, S.M. Rabiee, A.M. Goudarzi, M. Dardel, L. Tayebi, Optimization of composite bone scaffolds prepared by a new modified foam replica technique. Mater. Today Commun **31**, 103293 (2022). https://doi.org/10.1016/j.mtcomm.2022.103293
21. H.W. Kim, Y.J. Kim, Fabrication of strontium-substituted hydroxyapatite scaffolds using 3D printing for enhanced bone regeneration. J. Mater. Sci. **56**, 1673–1684 (2021). https://doi.org/10.1007/s10853-020-05391-y
22. L. Gritsch, M. Maqbool, V. Mouriño, F.E. Ciraldo, M. Cresswell, P.R. Jackson, A.R. Boccaccini, Chitosan/hydroxyapatite composite bone tissue engineering scaffolds with dual and decoupled

therapeutic ion delivery: copper and strontium. J. Mater. Chem. B **7**, 6109–6124 (2019). https://doi.org/10.1039/C9TB00897G
23. N. Monmaturapoj, W. Soodsawang, W. Thepsuwan, Porous hydroxyapatite scaffolds produced by the combination of the gel-casting and freeze drying techniques. J. Porous Mater. **19**, 441–447 (2012). https://doi.org/10.1007/s10934-011-9492-7
24. S.A.S. Nasrollah, N. Najmoddin, M. Mohammadi, A. Fayyaz, B. Nyström, Three dimensional polyurethane/hydroxyapatite bioactive scaffolds: the role of hydroxyapatite on pore generation. J. Appl. Polym. Sci. **138**, 50017 (2021). https://doi.org/10.1002/app.50017
25. S. Saber-Samandari, S. Saber-Samandari, S. Kiyazar, J. Aghazadeh, A. Sadeghi, In vitro evaluation for apatite-forming ability of cellulose-based nanocomposite scaffolds for bone tissue engineering. Int. J. Biol. Macromol. **86**, 434–442 (2016). https://doi.org/10.1016/j.ijbiomac.2016.01.102
26. M. Ramadas, G. Bharath, N. Ponpandian, A.M. Ballamurugan, Investigation on biophysical properties of hydroxyapatite/graphene oxide (HAp/GO) based binary nanocomposite for biomedical applications. Mater. Chem. Phys. **199**, 179–184 (2017). https://doi.org/10.1016/j.matchemphys.2017.07.001
27. D.O. Obada, K.A. Salami, A.N. Oyedeji, O.O. Fasanya, M.U. Suleiman, B.A. Ibisola, E.T. Dauda, Solution combustion synthesis of strontium-doped hydroxyapatite: effect of sintering and low compaction pressure on the mechanical properties and physiological stability. Mater. Lett. **304**, 130613 (2021). https://doi.org/10.1016/j.matlet.2021.130613
28. A.C. Mocanu, F. Miculescu, G.E. Stan, A.M. Pandele, M.A. Pop, R.C. Ciocoiu, L.T. Ciocan, Fiber-templated 3D calcium-phosphate scaffolds for biomedical applications: the role of the thermal treatment ambient on physico-chemical properties. Materials **14**, 2198 (2021). https://doi.org/10.3390/ma14092198
29. H. Ismail, M.N.Z. Zakri, H. Mohamad, A comparative study of physicomechanical and in vitro bioactivity properties of β-wollastonite/cordierite scaffolds obtained via gel casting method. Ceram. Int. **48**, 25495–25505 (2022). https://doi.org/10.1016/j.ceramint.2022.05.228
30. M. Arastouei, M. Khodaei, S.M. Atyabi, M.J. Nodoushan, The in-vitro biological properties of 3D printed poly lactic acid/akermanite composite porous scaffold for bone tissue engineering. Mater. Today Commun. **27**, 102176 (2021). https://doi.org/10.1016/j.mtcomm.2021.102176